JOURNAL OF AIRCRAFT
Vol. 44, No. 1, January–February 2007

Computational Analysis on Flow Through Transition *S*-Diffusers: Effect of Inlet Shape

K. Saha,* S. N. Singh,† and V. Seshadri‡
Indian Institute of Technology Delhi, New Delhi, Delhi 110 016, India
and
S. Mukhopadhyay§
Lingaya's Institute of Management & Technology, Faridabad, Haryana 122 002, India

DOI: 10.2514/1.22828

Diffusing transition *S*-ducts are often used in dual engine fighter aircrafts as intake ducts. The cross section shape at the inlet of the intake duct affects the performance of the duct. The present paper establishes computational fluid dynamics as a design tool for intake design. Various cross section shapes of the inlet, namely, elliptic, semicircular, oval, rectangular, and square, have been analyzed using the standard and the renormalized group k–ε turbulence model. For all the ducts, the angle of turn (22.5/22.5 deg), the centerline length (300 mm) and the circular exit diameter (100 mm) have been kept constant. Incompressible flow analysis has been done at 0.17 Mach number at the entry of the duct which corresponds to the throat of intakes. The elliptic-shaped inlet duct shows the best performance in terms of pressure recovery, loss coefficient, and flow distortion at the compressor face, whereas square duct produces the worst flow characteristics. It is also established that the renormalized group k–ε model predicts better than the standard k–ε turbulence model.

Nomenclature

C_L	=	total pressure loss coefficient, $(P_{\text{ti}} - P_t)/\frac{1}{2}\rho u_{\text{avi}}^2$
C_P	=	static pressure recovery coefficient, $(P_{\text{st}} - P_{\text{sti}})/\frac{1}{2}\rho u_{\text{avi}}^2$
$C_{\varepsilon 1}$, $C_{\varepsilon 2}$, C_μ	=	model constants
D_h	=	inlet hydraulic diameter
DC60	=	distortion coefficient in 60 deg sector, $(P_{\text{to}} - P_{60})/\frac{1}{2}\rho u_{\text{avo}}^2$
G	=	production term
I	=	turbulence intensity
k	=	turbulent kinetic energy, m^2/s^2
L	=	characteristic length
l	=	turbulence length scale, centerline length of the duct
P	=	pressure
P_{60}	=	total pressure at worst 60 deg sector of outlet
Pr_t	=	turbulent Prandtl number
$\bar{p}$	=	time-averaged static pressure
R	=	rate of strain
S_k, S_ε	=	user defined source terms for k and ε
S_m	=	mass added to continuous phase
u	=	velocity
$\bar{u}$	=	time-averaged velocity
x	=	longitudinal direction
x_i	=	tensorial notation of Cartesian coordinate system
α	=	inverse Prandtl number
δ_{ij}	=	Kronecker's delta
ε	=	turbulent kinetic energy dissipation rate, m^2/s^3
η	=	nondimensional parameter, Sk/ε
ν	=	molecular kinematic viscosity
ν_{eff}	=	effective kinematic viscosity
ν_t	=	turbulent or eddy kinematic viscosity
ρ	=	density of fluid
σ_k, σ_ε	=	Prandtl number for k and ε

Subscripts

avi	=	mass average property at inlet
avo	=	mass average property at outlet
i, j	=	tensorial notations
st	=	static property
sti	=	static property at inlet
t	=	stagnation property
to	=	stagnation property at outlet
ti	=	stagnation property at inlet
x, r	=	axial and radial directions for 2-D axisymmetric problems

Received 30 January 2006; accepted for publication 21 April 2006.

*Ph.D. Scholar
†Professor; sidhnathsingh@hotmail.com (Corresponding author)
‡Professor
§Assistant Professor; currently Assistant Professor, Mechanical Engineering Department, Kalyani Government Engineering College, Kalyani, Nadia, West Bengal 741 235, India.

I. Introduction

DIFFUSING transition *S*-ducts are used as intake ducts in dual engine fighter aircrafts such as Lockheed Tristar L-1011, General Dynamics F-16, McDonnel-Douglas F-18, etc. The functions of a well-designed diffusing duct are to decelerate the flow efficiently and increase the static pressure with minimal total pressure loss and distortion at compressor face of the engine. The *S*-shaped intake ducts invariably have circular outlet whereas inlet shape has to be made compatible with the fuselage shape and location. The inlet shape optimization for compatibility with the engine is one of the major issues in the *S*-duct design.

Over the years, computational fluid dynamics (CFD) has become a convenient tool to analyze complex 3-D flows as compared to time-consuming wind tunnel tests. A commercial CFD code, FLUENT [1], has been used to predict the flow in various transition ducts in the present study. The CFD code has been validated with the experimental data available in literature using both standard k–ε and renormalized group (RNG) k–ε turbulence models.

Guo and Seddon [2–4] have reported comprehensive experimental studies on rectangular to circular transition *S*-shaped diffusing ducts having offset either in horizontal plane or in both, namely, horizontal and vertical planes. They have also studied the effect of inlet swirl on the flow characteristics of these ducts. Many researchers, namely,

Anderson et al. [5], Taylor et al. [6], etc. have conducted experiments on *S*-shaped ducts of rectangular and circular cross sections with mild curvature (22.5/22.5 deg) using laser Doppler anemometry (LDA) for both laminar and turbulent flow. Their results also show the development of pressure-driven secondary motions with change in the direction of rotation in the second half as compared to the first half of the bend.

Ghia and Sukhey [7] have numerically established the generation of weak pair of vortices near the concave wall in the curved duct flow. Cheng and Farokhi [8] numerically predicted the flow within a *S*-shaped duct and compared their results with the experimental results of Butz [9] with reasonable success. A 3-D numerical solution for *S*-shaped diffuser by Majumdar et al. [10] compared reasonably well with the experimental results of Rojas et al. [11]. Harloff et al. [12,13] have carried out both experimental and numerical work as an extension of their earlier work (Smith et al. [14]) to establish the fully-elliptic Navier–Stokes (FNS) computer program, the PARC3D code for a 3-D duct geometry with strong secondary flows. They used Baldwin–Lomax [15] algebraic turbulence model with H–O type grid. Wellborn et al. [16] performed experimental and computational study on *S*-shaped diffusers for compressible flow. They have generated benchmark data to validate the computational codes for the intake duct designers. They have also validated FNS and parabolized Navier–Stokes (PNS) CFD codes with their experimental results with acceptable agreement. Berrier and Allan [17] have reported their experimental and computational studies on semicircular and semi-elliptical *S*-duct inlets for compressible flow analysis for the Mach number ranging from 0.25 to 0.83. They observed that the increase in the extent of boundary-layer ingestion with a distorted profile decreases the pressure recovery and increases the distortion. A detailed computational study using commercial CFD code FLUENT-6.1 [1] has been reported by Anand et al. [18] for circular *S*-shaped diffusers for incompressible flows at various Reynolds numbers, curvature ratios (ratio of radius of curvature of first bend to the second bend), and swirl at inlet. Their analysis has revealed improvement of performance parameters with the introduction of inlet swirl. They have also reported that the curvature ratio of 1.0 gives the best performance.

The emphasis of the present study is to establish the effect of inlet shape on the duct performance for incompressible flows. In the present study Mach number is 0.173 at the entry to the duct that corresponds to the throat of the intake. The approximation of incompressible airflow through the *S*-shaped ducts is quite acceptable for flow analysis as it represents satisfactory basis for estimating subsonic intake flow characteristics due to its simplicity in the governing equations (Seddon and Goldsmith [19]). In the present study, flow predictions using both the standard k–ε and the RNG k–ε models have been carried out. The paper is expected to provide useful information for the intake duct designers.

Table 1 Model constants in standard and RNG k–ε models (Biswas [20])

Models	C_μ	$C_{\varepsilon 1}$	$C_{\varepsilon 1}$	σ_k	σ_ε	β_0	η_0
Standard k–ε	0.09	1.44	1.92	1.0	1.3	——	——
RNG k–ε	0.0845	1.42	1.68	0.7179	0.0179	0.012	4.38

II. Mathematical Formulation and Numerical Technique

The present simulations have been performed using the general purpose CFD code FLUENT [1] based on finite volume approach. The basic governing equations used are as follows (Biswas [20]).

Continuity equation:

$$\frac{\partial \bar{u}_i}{\partial x_i} = 0 \tag{1}$$

Momentum equation:

$$\frac{\mathrm{D}\bar{u}_j}{\mathrm{D}t} = -\frac{\partial(\bar{p} + 2k/3)}{\partial x_j} + \frac{\partial}{\partial x_i}\left[\nu_t\left(\frac{\partial \bar{u}_i}{\partial x_j} + \frac{\partial \bar{u}_j}{\partial x_i}\right)\right] \tag{2}$$

ν_t can be expressed empirically as

$$\nu_t = C_\mu \frac{k^2}{\varepsilon} \tag{3}$$

For closure solution, some additional equations are required to solve for the unknown parameter ν_t. In the present analysis, the standard k–ε and RNG k–ε two-equation turbulence models have been used.

The standard k–ε model (Launder and Spalding [21]) consists of two equations, one for the turbulent kinetic energy and the other for the turbulence dissipation rate to evaluate ν_t as follows.

Turbulent kinetic energy equation:

$$\frac{\mathrm{D}k}{\mathrm{D}t} = \frac{\partial}{\partial x_j}\left[\frac{\nu_t}{\sigma_k}\frac{\partial k}{\partial x_j}\right] + G - \varepsilon \tag{4}$$

Turbulence dissipation rate equation:

$$\frac{\mathrm{D}\varepsilon}{\mathrm{D}t} = C_{\varepsilon 1}\frac{\varepsilon}{k}G + C_{\varepsilon 2}\frac{\varepsilon^2}{k} + \frac{\partial}{\partial x_j}\left[\frac{\nu_t}{\sigma_\varepsilon}\frac{\partial \varepsilon}{\partial x_j}\right] \tag{5}$$

The production term is defined as

$$G = \nu_t\left(\frac{\partial \bar{u}_i}{\partial x_j} + \frac{\partial \bar{u}_j}{\partial x_i}\right)\frac{\partial \bar{u}_i}{\partial x_j} \tag{6}$$

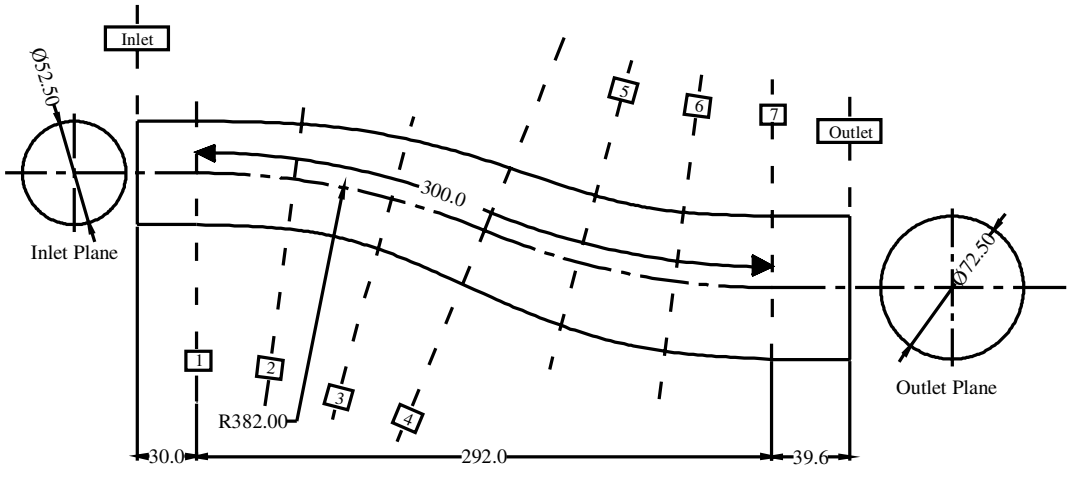

Plane	Angle of Turn
1	0 deg
2	7.5 deg
3	15 deg
4	22.5 deg/-22.5 deg
5	-15 deg
6	-7.5 deg
7	0 deg

All dimensions are in mm.

Fig. 1 Schematic layout of the *S*-duct used for validation of CFD code (Anand et al. [23]).

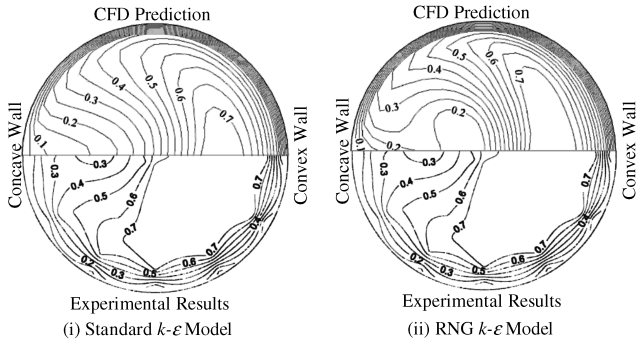

a) Normalized Mean Velocity Contour Comparison on Plane-7

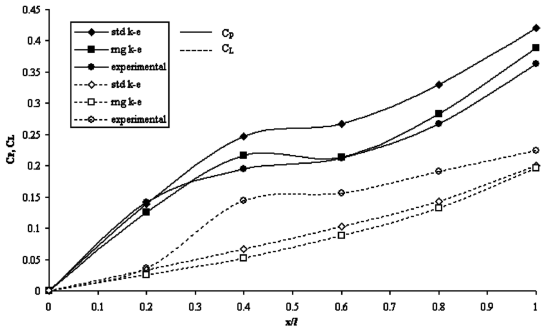

b) Static Pressure Recovery and Total Pressure Loss Coefficient Comparison along the Centerline Length

Fig. 2 Validation of CFD code with the experimental results of Anand et al. [23].

RNG k–ε model provides a more generalized and fundamental model with useful modification for swirl flows. It also provides improved prediction for separated flows, flow over curved geometries, etc. In this model the governing equations are derived using the mathematical technique called "renormalized group" method due to Yakhot and Orszag [22]. The modified k- and ε-equations are as follows.

k-equation:

$$\frac{\mathrm{D}k}{\mathrm{D}t} = \frac{\partial}{\partial x_j}\left(\alpha \nu_t \frac{\partial k}{\partial x_j}\right) - \varepsilon + \nu_t S^2 \tag{7}$$

ε-equation:

$$\frac{\mathrm{D}\varepsilon}{\mathrm{D}t} = C_{\varepsilon 1}\frac{\varepsilon}{k}\nu_t S^2 - C_{\varepsilon 2}\frac{\varepsilon^2}{k} - R + \frac{\partial}{\partial x_j}\left(\alpha \nu_t \frac{\partial \varepsilon}{\partial x_j}\right) \tag{8}$$

The RNG model extends the prediction of effective viscosity beyond the high Reynolds number limit and it is modified in terms of k and ε such that it allows the model to predict low Reynolds number and near-wall flows.

$$\nu_{\mathrm{eff}} = \nu\left[1 + \sqrt{\frac{C_\mu}{\nu}}\frac{k}{\sqrt{\varepsilon}}\right] \tag{9}$$

The effective viscosity is defined as $\nu_{\mathrm{eff}} = \nu + \nu_t$.

The rate of strain term is given as

$$R = 2\nu_t S_{ij}\overline{\frac{\partial u_i}{\partial x_i}\frac{\partial u_i}{\partial x_j}} \tag{10}$$

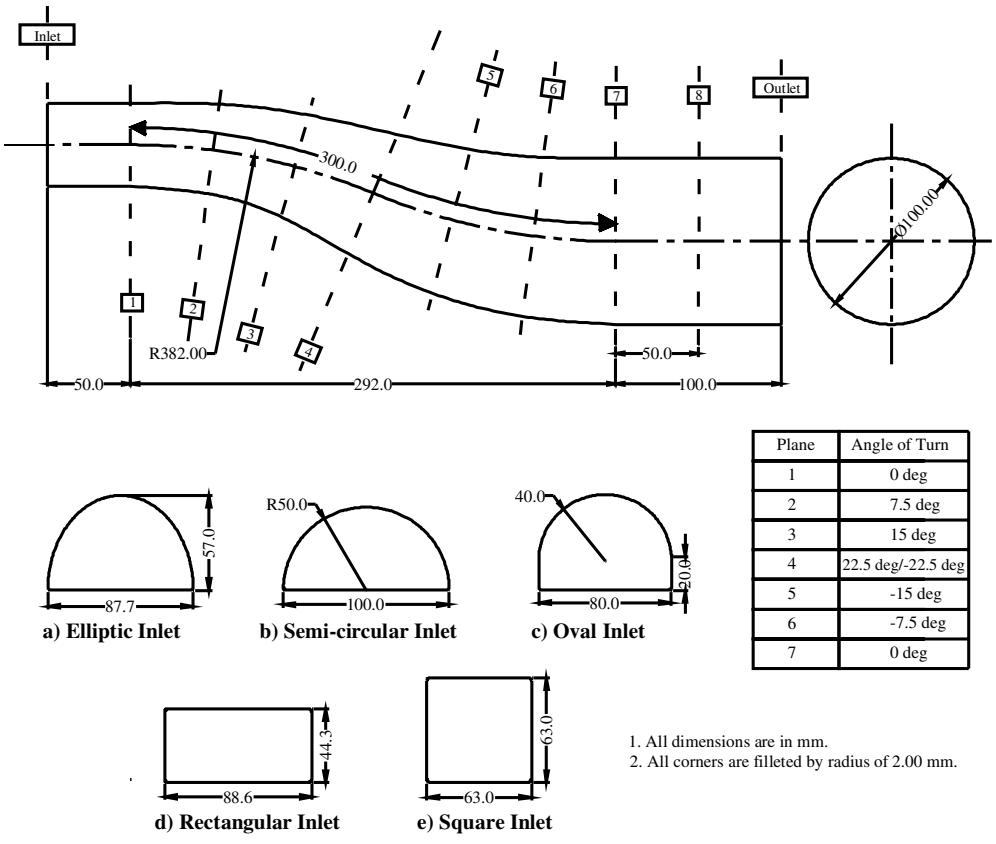

Plane	Angle of Turn
1	0 deg
2	7.5 deg
3	15 deg
4	22.5 deg/-22.5 deg
5	-15 deg
6	-7.5 deg
7	0 deg

1. All dimensions are in mm.
2. All corners are filleted by radius of 2.00 mm.

Fig. 3 Schematic layout of various transition ducts.

This term in RNG k–ε model is expressed as

$$R = \frac{C_\mu \eta^3 (1 - \eta/\eta_0)}{1 + \beta \eta^3} \frac{\varepsilon^2}{k} \tag{11}$$

where $S^2 = 2S_{ij}S_{ij}$.

The inverse Prandtl number can be expressed as (Yakhot and Orszag [22])

$$\left|\frac{\alpha - 1.3929}{\alpha_0 - 1.3929}\right|^{0.6321} \left|\frac{\alpha + 2.3929}{\alpha_0 + 2.3929}\right|^{0.3679} = \frac{\nu}{\nu_{\text{eff}}}$$

where $\alpha_0 = 1$. For high Reynolds number, fully developed turbulent flow, $\alpha = 1.3929$ and the turbulent Prandtl number is 0.7179. For the sake of completeness, the values of the various constants in the two turbulence models are given in Table 1.

The discretization procedure for the 3-D solution domain has been performed with the help of an inbuilt solid modeling and meshing tool with FLUENT, called GAMBIT. It employs body-fitted nonorthogonal grid system. Hexahedral meshing was done along with the growth factor in the normal direction to the wall. The growth of the mesh size helps to get finer mesh near the wall as well as coarser mesh away from the wall. The number of elements used for all the ducts was of the order of 150,000. Wall function approach (Spalding and Launder [21]) has been adopted for the near-wall treatment as it is computationally economical for high Reynolds number flows, robust and reasonably accurate (FLUENT [1]). The governing equations have been integrated over the control volume and discretized by second order upwind scheme. Also the governing equations have been linearized implicitly. Pressure-velocity coupling has been done using the SIMPLE algorithm. A point implicit (Gauss–Seidel) linear equation solver has been used in conjunction with an algebraic multigrid (AMG) method to solve the resultant scalar system of equations for the dependent variable in each cell. The residuals and mass weighted average velocity at exit plane have been monitored to check the convergence of the solution. The convergence criteria for the residuals were set at 1×10^{-8}. The computations have been carried out in a Windows based Pentium-4 workstation with 2 Gb RAM. It took on an average 4 h for each solve.

III. Validation of CFD Code

A preliminary investigation has been done to validate the CFD code with the experimental data of Anand et al. [23] in a 22.5/22.5 deg S-shaped circular diffuser (Fig. 1) with an l/d ratio of 5.7. This geometry was modeled to predict the flow using the two turbulence models, namely, standard k–ε and RNG k–ε model with the experimentally measured inlet velocity profile as input. The geometry modeled had a uniform wall roughness of 0.8 mm and the same has been specified in the boundary condition.

Figure 2a (i and ii) shows the comparison between experimental and computational normalized mean velocity contours for the standard k–ε model and the RNG k–ε model at Plane-7. The standard k–ε model predicts smaller high velocity core towards the convex wall compared with the RNG model, whereas experimental contour shows larger high velocity contour near the same wall. The RNG k–ε model shows the formation of low velocity core towards the concave wall side, which is in very close agreement with the experimental results. Comparison of longitudinal static pressure recovery and total pressure loss coefficients are shown in Fig. 2b. The RNG k–ε model predicts C_P of 38.9%, which is close to the experimental results ($C_P = 36.4\%$), whereas the standard k–ε model predicts 42.1%. The loss coefficient values predicted by both the models are nearly identical. It is also seen that the deviation between experiments and predictions is quite large at the inflexion region, highlighting the failure of turbulence models to predict the flow in regions of steep velocity gradients.

The analyses carried out for validation with the two turbulence models illustrate good matching of the global performance parameters with the experimental results. A closer look at the validation results shows that the RNG k–ε model gives better agreement with the experimental results as also reported in the literature (Choudhury [24]). Calculations of error in predicted velocities, assuming experimental results to be accurate, gave a value of about 12% for the standard k–ε model whereas it was of the order of 8% with the RNG k–ε model. Similarly it is seen that the error in predicted overall pressure recovery coefficient is around 15% for the standard k–ε turbulence model whereas it is around 7% with RNG k–ε turbulence model.

IV. Geometries Investigated

To establish the effect of inlet shape on the performance of S-shaped diffusing transition intake ducts, the following inlet shapes, namely, elliptic, oval, semicircular, rectangular, and square as shown in Fig. 3 have been analyzed using air as the fluid. The following geometrical parameters for the ducts were kept constant:

1) Area ratio: 2.0
2) Centerline length: 300 mm
3) Angle of turn: 22.5/22.5 deg
4) Outlet diameter: 100 mm

A constant area duct having length equal to one outlet diameter was provided at the end of the curved diffusing duct and another

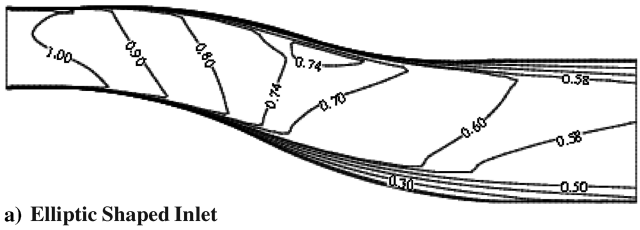

a) Elliptic Shaped Inlet

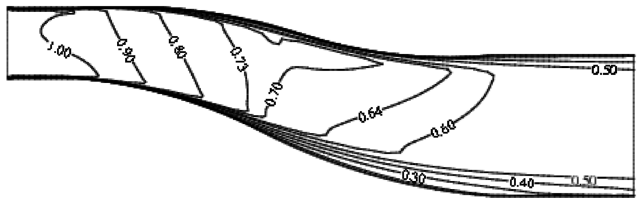

b) Semi-circular Shaped Inlet

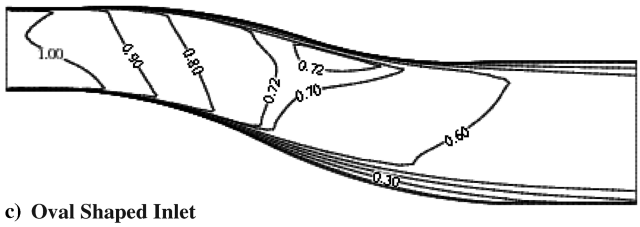

c) Oval Shaped Inlet

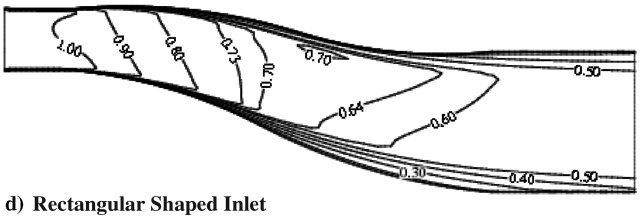

d) Rectangular Shaped Inlet

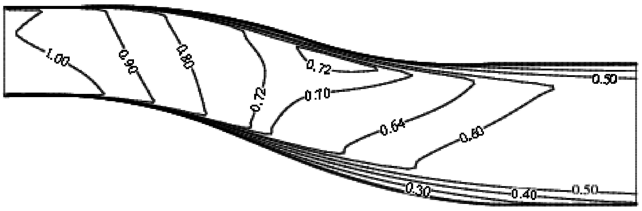

e) Square Shaped Inlet

Fig. 4 Normalized mean velocity contour on the longitudinal midplane.

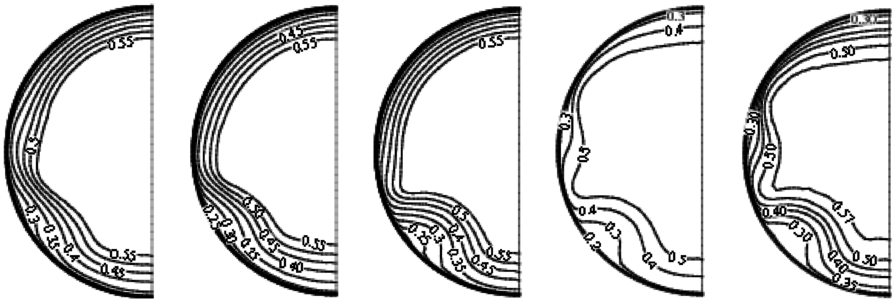

a) Elliptic Shaped Inlet | b) Semi-circular Shaped Inlet | c) Oval Shaped Inlet | d) Rectangular Shaped Inlet | e) Square Shaped Inlet

Fig. 5 Normalized mean velocity contour at exit plane.

constant area duct having length equal to 50 mm was provided ahead of the inlet of the transition duct.

V. Boundary Conditions

The CFD simulation for *S*-shaped transition intake ducts has been carried out for uniform velocity (60 m/s) at the inlet considering half model due to geometrical similarity about the horizontal central plane. Symmetric boundary condition was specified on this plane. Zero gauge pressure was specified as outlet condition for all the ducts for evaluation of comparative performance. To specify the turbulence quantities, namely, the turbulent kinetic energy and turbulence dissipation rate, the following relationship is used:

$$k = \frac{3}{2}(u_{\text{av}} I)^2 \tag{13}$$

and

$$\varepsilon = C_\mu^{3/4} \frac{k^{3/2}}{l} \tag{14}$$

where $l = 0.07L$.

The turbulence intensity at the exit was obtained by the relation

$$I = 0.16(Re)^{-1/8} \tag{15}$$

where Re is the Reynolds number based on the hydraulic diameter. The inlet turbulence intensity was set at 0.5%. No-slip boundary condition has been specified at the duct walls. The standard wall function has been chosen for the near-wall treatment. The y^+ values for all the cases have been checked to be of the order of 200, whereas for the standard wall function treatment range of the y^+ value is $30 < y^+ < 300$. This implies that the selection of the standard wall function treatment is acceptable.

VI. Results and Discussion

The nondimensionalized computational results in terms of the mean velocity contours, crossflow velocity contours, static pressure recovery, and total pressure loss coefficient and distortion coefficient (DC60) have been presented in Figs. 4–8 and Table 2. The velocity and pressure parameters have been normalized by inlet mass averaged velocity and the inlet dynamic pressure, respectively.

A. Mean Velocity Contours

The normalized mean velocity contours at the longitudinal mid plane for all transition ducts are presented in Fig. 4. An overall observation of the contours shows the flow development to be similar for all the ducts. Velocity contours show high velocity close to convex wall and low velocity at the concave wall for both the bends. Velocity contours also show continuous diffusion along the longitudinal length. Figure 5 shows the mean velocity contours at the exit plane (Plane-8). The contours show nonuniformity near the concave wall side. It is clearly seen that elliptic- and semicircular-shaped inlet ducts produce better flow uniformity at the exit whereas square-shaped inlets show the worst flow uniformity.

B. Secondary Flow Velocity Vectors

The normalized secondary velocity contours plotted in Fig. 6 show the formation of a pair of counter-rotating vortices which have a tendency to break into more numbers of weak vortices with the square-shaped inlet duct having the strongest secondary motion [Fig. 6e].

C. Performance Parameters

The variation of performance parameters (C_P and C_L) for different transition ducts along the longitudinal length are presented in Figs. 7 and 8 respectively.

1. Static Pressure Recovery Coefficient

Figure 7 depicts a monotonic growth in pressure recovery along the normalized length where the longitudinal length has been normalized by the total centerline length of the duct (l). The overall pressure recovery ($C_P \approx 66\%$) is nearly same for all ducts. A mild kink is seen for all the ducts near the inflexion plane, due to change in centerline curvature. The maximum C_P value achieved is 67.37% for semicircular duct.

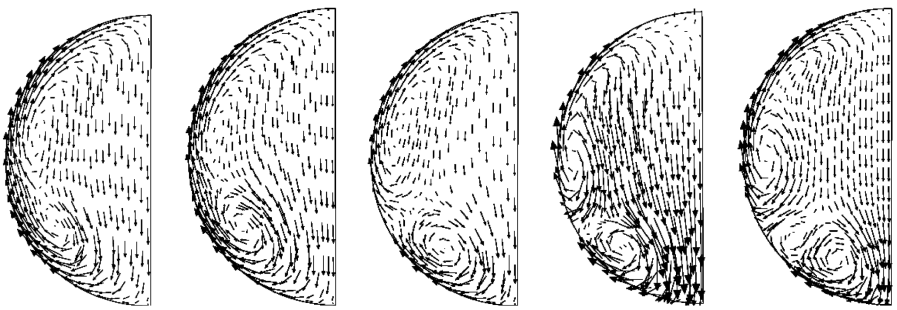

a) Elliptic Shaped Inlet | b) Semi-circular Shaped Inlet | c) Oval Shaped Inlet | d) Rectangular Shaped Inlet | e) Square Shaped Inlet

Fig. 6 Normalized crossflow velocity vectors at exit plane.

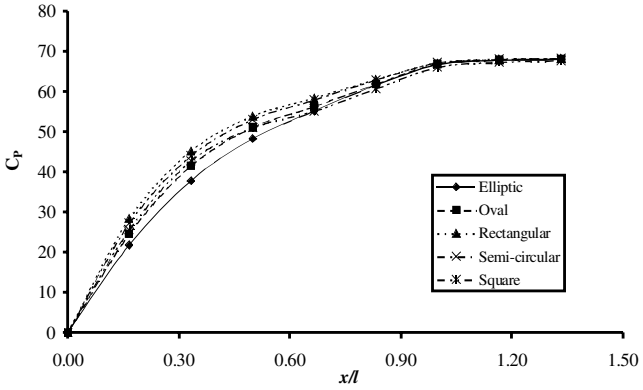

Fig. 7 Static pressure recovery coefficient.

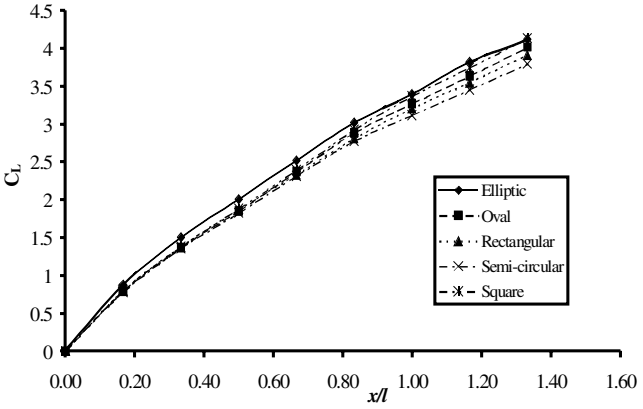

Fig. 8 Total pressure loss coefficient.

2. Total Pressure Loss Coefficient

The total pressure loss coefficient increases almost linearly along the longitudinal length (Fig. 8). The overall loss coefficient for the square-shaped inlet duct is maximum (4.13%) whereas for the semicircular duct it is minimum (3.79%).

3. Distortion Coefficient in 60 deg Sector

One of the most important parameters to judge the performance of the intake ducts is the distortion coefficient. Table 2 gives the DC60 values for various ducts. The elliptic inlet shape duct has the least DC60 value (0.032) followed by semicircular duct (DC60 = 0.053). The DC60 for the square inlet is 0.149. Therefore, from the DC60 values, it can be concluded that elliptic inlet gives the best uniformity in terms of total pressure distortion at the exit of the *S*-diffusing duct.

VII. Conclusions

The present computational study has been carried out on different transition *S*-ducts based on two turbulence models. The following conclusions have been drawn from the study:

1) Validation of the CFD code shows that the RNG k–ε turbulence model gives better prediction compared with the standard k–ε turbulence model. This may be due to the superior capability of RNG k–ε model to pick up the transverse pressure gradients in the ducts having streamline curvature (Choudhury [24]).

Table 2 Transition *S*-duct performance

Inlet shapes	C_P	C_L	DC60
Elliptic	66.42	4.11	0.032
Semicircular	67.37	3.79	0.053
Oval	66.80	4.01	0.103
Rectangular	66.93	3.91	0.093
Square	66.21	4.13	0.149

2) The performance parameters, as shown in Table 2, depict that the semicircular inlet duct has the best performance followed by the elliptic shaped inlet duct on the basis of C_P and C_L values, whereas elliptic inlet duct shows the least total pressure distortion at the exit (DC60 = 0.032).

3) The square-shaped duct has the worst performance among all the transition *S*-ducts investigated. The distortion coefficient values (DC60) for different ducts (Table 2) depict the square duct to produce the most distorted flow (DC60 = 0.149). The maximum exit flow distortion for square duct is also supported by the mean velocity contours and the crossflow velocity vector plots in the transverse planes near the exit [Figs. 5e and 6e].

References

[1] Fluent, User's Guide, CFD Software Package, Ver. 6.2, Fluent, Lebanon, NH, 2005.

[2] Guo, R. W., and Seddon, J., "An Investigation of the Swirl in an *S*-Duct," *Aeronautical Quarterly*, Vol. 33, May 1982, pp. 25–58.

[3] Guo, R. W., and Seddon, J., "Swirl Characteristics of a *S*-Shaped Air Intake with Both Horizontal and Vertical Offsets," *Aeronautical Quarterly*, Vol. 34, May 1983, pp. 130–146.

[4] Guo, R. W., and Seddon, J., "The Swirl in an *S*-Duct of Typical Intake Proportions," *Aeronautical Quarterly*, Vol. 34, May 1983, pp. 99–128.

[5] Anderson, B. H., Taylor, A. M. K. P., Whitelaw, J. H., and Yianneskis, M., "Developing Flow in *S*-Shaped Ducts," *Proceedings of the 2nd International Symposium on the Application of LDA to Fluid Mechanics*, Ladoan, Instituto Supervior Technico, Lisbon, Portugal, 1982, pp. 4.2.1–4.2.17.

[6] Taylor, A. M. K. P., Whitelaw, J. H., and Yianneskis, M., "Developing Flow in *S*-Shaped Ducts, Part 2—Circular Cross-Section Duct," NASA-CR-3759, Feb. 1984.

[7] Ghia, K. N., and Sukhey, J. S., "Laminar Incompressible Viscous Flow in Curved Ducts of Regular Cross-Sections," *Journal of Fluids Engineering*, Vol. 99, No. 4, 1977, pp. 640–648.

[8] Cheng, G. C., and Farokhi, S. "On Turbulent Flows Dominated by Curvature Effects," *Journal of Fluids Engineering*, Vol. 114, No. 1, 1992, pp. 52–57.

[9] Butz, L. A., "Turbulent Flow in *S*-Shaped Ducts," M.Sc. Thesis, Purdue Univ., West Lafayette, IN, 1979.

[10] Majumder, S., Rodi, W., and Zhu, J., "Three-Dimensional Finite-Volume Method for Incompressible Flows with Complex Boundaries," *Journal of Fluids Engineering*, Vol. 114, No. 4, 1992, pp. 496–503.

[11] Rojas, J, Whitelaw, J. H., and Yianneskis, M., "Developing Flow in *S*-Shape Diffuser, Part 2, Circular Cross-Section Diffuser," Dept. of Mechanical Engineering, Imperial College of Science and Technology, Pub. No. FS/83/28, 1983.

[12] Harloff, G. J., Reichert, B. A., and Wellborn, S. R., "Navier-Stokes Analysis and Experimental Data Comparison of Compressible Flow in a Diffusing *S*-Duct," NASA Technical Memorandum 105683; also AIAA Paper 92-2699, 1992.

[13] Harloff, G. J., Smith, C. F., Burns, J. E., and DeBonis, J. R., "Navier-Stokes Analysis of 3-D *S*-Ducts," *Journal of Aircraft*, Vol. 30, No. 4, 1993, pp. 526–533.

[14] Smith, C. F., Bruns, J. E., Harloff, G. J., and Debonis, J. R., "Three-Dimensional Compressible Turbulent Computations for a Diffusing *S*-Duct," NASA CR 4392, 1991.

[15] Baldwin, B. S., and Lomax, H., "Thin Layer Approximation and Algebraic Mode for Separated Turbulent Flows," AIAA, Paper 78-257, 1978.

[16] Wellborn, S. R., Okiishi, T. H., and Reichert, B. A., "A Study of the Compressible Flow Through a Diffusing *S*-Duct," NASA-TM-106411, Dec. 1993.

[17] Berrier, B. L., and Allan, B. G., "Experimental and Computational Evaluation of Flush-Mounted, *S*-Duct Inlets," AIAA Paper 2004-0764, 2004.

[18] Anand, R. B., Rai, L., and Singh, S. N., "Flow Characteristics of Short and Long *S*-Shaped Diffusers: Effect of Reynolds Number Curvature Ratio and Swirl," *International Journal of Computational Fluid Dynamics*, Vol. 14, No. 4, 2005, pp. 191–203.

[19] Seddon, J., and Goldsmith, E. L., *Inlet Aerodynamics*, Blackwell Science, Boston, MA, 1999.

[20] Biswas, G., "The k–ε Model, the RNG k–ε Model and the Phase-Averaged Model," *Turbulent Flows: Fundamentals, Experiments and Modeling*, edited by G. Biswas and V. Eswaran, IIT Kanpur Series of

Advanced Texts, Narosa Publicating House, India, 2002.
[21] Launder, B. E., and Spalding, D. B., "The Numerical Computation of Turbulent Flows," *Computer Methods in Applied Mechanics and Engineering*, Vol. 3, 1974, pp. 269–289.
[22] Yakhot, V., and Orszag, S. A., "Renormalization Group Analysis of Turbulence: 1. Basic Theory," *Journal of Scientific Computing*, Vol. 1, No. 1, 1986, pp. 1–51.
[23] Anand, R. B., Rai, L., and Singh, S. N., "Performance Characteristics of a 22.5°/22.5° *S*-Shaped Circular Diffuser with and Without Swirl," *Journal of Mechanical Engineering Research and Developments*, (to be published).
[24] Choudhury, D., "Introduction to the Renormalization Group Method and Turbulence Modeling," Fluent Technical Memorandum TM-107, Lebanon, NH1993.